Temporal variations of coda *Q*: an attenuation-coefficient view

Igor B. Morozov

Department of Geological Sciences, University of Saskatchewan, Saskatoon, SK S7N 5E2 Canada

Igor.Morozov@usask.ca

Abstract

Spatial and temporal variations of coda wave attenuation were identified in many studies, and particularly in relation to major earthquakes and volcanic eruptions. Both the coda quality factor, Q_c, and its frequency dependence often change following such events, which is often attributed to variations in the properties of large volumes of the subsurface. However, Q_c is also strongly sensitive to the assumed theoretical models, which are usually insufficiently accurate for constraining the actual relationships between the geometrical spreading, anelastic dissipation, and scattering. This inaccuracy often leads to significant exaggeration of attenuation effects and complicates the interpretation of temporal variations. To resolve this problem, this study uses a phenomenological approach based on the temporal attenuation coefficient χ instead of Q_c. The attenuation coefficient often linearly depends on frequency f, with intercept $\gamma = \chi(0)$ related to the geometrical spreading and slope giving the "effective quality" factor Q_e as $d\chi/df = \pi Q_e^{-1}$. Two published examples of temporal variations of local-earthquake coda are revisited: a non-volcanic (Stone Canyon in central California) and volcanic area (Mt. St. Helens,

Washington). In both cases, linear $\chi(f)$ patterns are found, with the effects of γ on coda decay rates being significantly stronger than those of Q_e^{-1}. At Stone Canyon, γ ranged from 0.035 to 0.06 s^{-1} and Q_e varied from 3000 to 10,000, with γ increasing and Q_e decreasing during the winter season. At Mt. St. Helens, γ remained constant at ~0.18 s^{-1}, and Q_e changed from 400 before the eruption to 750 after it. The observed temporal variations are explained by the near-surface changes caused by seasonal variations in the non-volcanic case and gas-, magma-, and geothermal-system related in the volcanic case. Scattering attenuation does not appear to be a significant factor in these areas, or otherwise it may be indistinguishable due to its fundamental trade-off with the background structure and anelastic attenuation in the data.

Key words: seismic coda; attenuation; scattering; *Q*; lithosphere.

1. Introduction

Measurements of seismic-coda attenuation provide critical information about the physical state of the Earth's interior. Due to its averaging over significant volumes of the lithosphere and multiple wave types, coda provides good stability of estimates and allows detection of small temporal variations in seismic attenuation related to the volcanic activity or environmental changes. However, the association of the measured quantity, which is usually the frequency-dependent coda "quality" factor, Q_c (Aki, 1980) with the *in situ* physical properties is not straightforward and may be prone of uncertainties and pitfalls. The apparent Q_c is conventionally inverted for the *in situ* elastic (scattering, Q_s) and anelastic (intrinsic, Q_i) quality factors, which are associated with the properties of velocity/density fluctuations and anelastic energy dissipation, respectively (*e.g.*, Jin and Aki, 1986; Aki, 1991). This inversion is usually based on the single-scattering (Aki and Chouet, 1975) or multiple-scattering models (*e.g.*, Dainty and Toksöz, 1977; Fehler *et al.*, 1992). All of these models use a number of strong assumptions and simplifications, such as the uniform or smooth velocity background, perfectly-known geometrical spreading (GS), absence of free-surface effects and layered reflectivity, and isotropic and often uniformly-distributed scattering. However, these assumptions are inaccurate in most observational situations, and their inaccuracy may account for the entire frequency dependence of Q_c and lead to strong (up to 20–30 times) differences between the apparent and the *in situ* Q^{-1} values (Morozov, 2008, 2009a, b).

The sensitivity of the frequency-dependent seismic Q to GS corrections is well known (*e.g.*, Kinoshita, 1994). Broad acceptance of several standard reference models for

GS, such as $G(t) = t^{-1}$ for local-earthquake body waves (here and below, t is the travel time and f is the frequency) allows comparisons between the $Q_c(f)$ dependencies derived for different areas or time intervals. However, this abstract reference reduces such dependencies to descriptions of coda amplitudes and not necessarily of the Earth's physical properties. For an unbiased interpretation of the *in situ* Q, measurements should be conducted so that the results are independent of GS variations and model assumptions.

Recently, we suggested that the uncertainties caused by the GS *versus* $Q(f)$ trade-off can be removed if instead of using the quality factor Q, we return to interpreting the temporal attenuation coefficient, χ (which was denoted α in Morozov, 2008). This attenuation coefficient incorporates the variations of GS and is directly measured in most observations. It was also modeled numerically (Morozov *et al*., 2008) and correlated to geological structures and tectonic ages (Morozov, 2008). The $\chi(f)$ parameterization of the seismic-amplitude data is stable in respect to the selection of background models, and the trade-off with GS assumptions is only introduced after its transformation to the quality factor as $Q = \pi f/\chi$. Note that this transformation also leads to Q often increasing with frequency (up to $Q \propto f$) when the zero-frequency limit $\chi|_{f \to 0}$ is non-zero and positive (Morozov, 2008, 2009a, 2010a). Such increases in local-coda $Q(f)$ were reported in many studies.

In all data cases considered so far (Morozov, 2008, 2009a, 2010a, and b), the use of χ simplified the interpretation and revealed data relationships that would be hard to notice in the form of Q. A general observation from these studies is that χ often shows a linear dependence on f with a non-zero limit $\gamma = \chi|_{f=0}$, which suggests its presentation in

the general form

$$\chi(f) = \gamma + \frac{\pi}{Q_e(f)} f \,. \tag{1}$$

Here, γ can be interpreted as the residual GS, and Q_e is the "effective attenuation" quality factor (Morozov, 2008). Because of their distinct roles in both the observable frequency dependencies of χ and also in theory, coordinates (γ, Q_e) often lead to broader and clearer separation between different observations than parameters Q_0, and η of the commonly used power law $Q(f) = Q_0 f^{\eta}$.

In this paper, we use the attenuation-coefficient concept to revisit two observations of temporal variations of local-earthquake coda attenuation. Many authors reported local-earthquake coda attenuation (Q_c) varying over time scales from several weeks to a few years, such as Chouet (1976, 1979), Aki (1980), Stewart *et al*. (1983), Rhea (1984), Novelo-Casanova *et al*. (1985), Sato (1986), Jin and Aki (1986), Peng *et al*. (1986), Sato (1986), Fehler *et al*. (1988), Londono (1996), Gusev (1997), Del Pezzo *et al*. (2004), Moncayo *et al*. (2004), Novelo-Casanova *et al*. (2006). The results were invariably interpreted by using the single- and multiple-scattering coda models, *i.e*. by inverting Q_c in terms of the *in situ* Q_s and Q_i.. Accordingly, the observed temporal variations of Q_c were attributed to the crustal heterogeneity and dissipation changing as a result of the seasonal or volcanic activities. Whereas not all of these observations were equally convincing, the very first of them (Chouet, 1979; Aki, 1980) presented a spectacular Q_c variation recorded continuously for over about a year of an extensive aftershock study in central California. This study was also sufficiently detailed and well-documented in order to attempt reproducing a part of its χ data in this paper.

Re-examination of the data by Chouet (1979) shows that the $\chi(f)$ picture (1) offers a different and a simple perspective on the observed temporal variations. As shown below, $\chi(f)$ retains its linear character during the different periods of observations, with both γ and Q_e values changing with time. Contrary to what is commonly assumed, the "material" attenuation (the part of *in situ* attenuation which vanishes at $f = 0$; see *Discussion* below) in this case plays a relatively minor role in the observed coda. This attenuation is responsible for only about one third of the recorded energy dissipation rate at the highest frequencies. The main effect, including the observed temporal variation of the apparent Q_c, belongs to γ, *i.e*., to changes in the velocity/density structure. Realization of this fact leads us to emphasizing the near-surface effects, by contrast to the very strong (several per cent of r.m.s. velocity fluctuations) and rapid (within a week) variations of velocity heterogeneity within a large volume (tens of kilometres radius) of the lithosphere inferred by Aki (1980).

In many studies, temporal variations of coda Q_c were studied at volcanoes (*e.g*., Chouet, 1976; Fehler *et al*., 1988; Londono, 1996; Moncayo *et al*., 2004, Novelo-Casanova *et al*., 2006; Del Pezzo *et al*. 2004). In these cases, the key observed coda characteristics are usually the temporal variations of the values of Q_c at selected frequencies and also the dependencies of Q_c on frequency. To illustrate this case, we briefly revisit the data from 1981 Mount St. Helens eruption by Fehler *et al*. (1988). Similarly to the study by Chouet (1979), this dataset also contains clear (but different) temporal and frequency-dependent effects, allows comparing the GS and Q^{-1} contributions, and leads to interesting observations of their variations during the process of volcanic activity.

By contrast to non-volcanic regions where strong frequency dependencies with $\eta \approx 1$ are common (*e.g.*, Roecker *et al*. 1982), frequency dependencies of the volcanic Q_c vary from weak (Chouet, 1976; Fehler *et al*., 1988) to strong (*e.g*., Londono, 1996; Moncayo *et al*., 2004). No widely accepted theory exists to explain these variations, and particularly the weak frequency dependence of Q_c at volcanoes. Aki (1980) suggested that in the presence of magma, the anelastic attenuation could be predominant and leading to a frequency-independent Q^{-1} within the seismic band, whereas scattering should generally cause Q^{-1} to decrease with increasing frequency (Dainty, 1981). Roecker *et al*. (1982) also suggested that Q_c strongly depends on the depth of sampling by the scattered waves, which was inferred from coda lag times.

However, note that the above contrasting of the scattering- to anelastic-Q and frequency-independent to frequency-dependent Q_c relies entirely on the selected theoretical models, for which the single- or multiple-scattering models are used in most cases. Without these models, even the definition of scattering Q becomes uncertain, and its frequency dependence changes dramatically when different models are considered (Morozov, 2008, 2009a, 2010a). Although giving a convenient framework for comparing the observations by reducing them to some *in situ* Q_i and Q_s, scattering models are based on so strongly simplified assumptions that they should lead to a fairly distorted physical picture of coda attenuation. In this picture, the residual GS is presented as an enigmatic frequency-dependence of Q_s, Q_i^{-1} may be significantly over-estimated, the significance of scattering is exaggerated, and scatterers themselves are broadly distributed within the lithosphere instead of being concentrated closer to the surface or fault zones as the geology usually suggests. This picture should be particularly problematic in volcanic

environments, where contrasting surface topography and extreme subsurface heterogeneity are abundant.

Unfortunately, in the conventional practice, reliance on grossly inaccurate models affects not only the interpretation but even the initial data presentation. Coda attenuation data are typically shown in the form of Q_c^{-1}, which is obtained by subtracting the theoretical GS prediction from the log-amplitude data (which corresponds to the χ_c) and dividing by the frequency. It appears that by returning to the phenomenological attenuation coefficient χ_c, the model-related GS artefact can be "undone," and comparisons of the observed coda properties become reliable. The results of this simple transformation are quite impressive. Even in the two well-known datasets mentioned above, this approach leads to several observations that were not visible in the Q_c picture.

2. Attenuation coefficient and Q

The attenuation-coefficient view on seismic attenuation (Morozov, 2008, 2010a, b, d) starts from a generalization of the classic scattering-theory approximation (Chernov, 1960; Sato, 1978) and further extends into a critique of the concept of Q and the theory of viscoelasticity (Morozov, 2009c, 2010c). Currently, this approach is undergoing some debate (Morozov, 2009a, b; Xie and Fehler, 2009; Mitchell, 2010; Xie, 2010). The approach is based on three key observations. First, we note that neither the observed (apparent) nor *in situ* (material) Q are defined as independent quantities, but both of these quality factors arise from the corresponding "temporal attenuation coefficients," which we denote χ:

$$Q^{-1} = \frac{\chi}{\pi f} \ . \tag{2}$$

Note that χ is measured in frequency units. In attenuation measurements, χ is the observable property arising from the logarithmic decrement of the seismic amplitude decay: $A(t) \propto \exp(-\chi t)$, or from the widths of spectral peaks of free oscillations. In forward modeling and inversion, χ is the imaginary part of the complex frequency, and therefore it also represents the primary quantity. The quality factor Q is only subsequently derived from χ by using eq. (2).

Second, theoretically, the attenuation coefficient χ arises from the fundamental scattering-theory approximation for seismic amplitudes:

$$P = G_0 e^{-\chi t} , \tag{3}$$

where P is the path factor (seismic amplitude corrected for source and receiver effects) and G_0 is some reference "GS," which is the value of P predicted for the best-known structure in the absence of attenuation and normalized so that $G_0 = P|_{t=0}$. It this equation, quantities χ, G_0, and P may depend on time, frequency, and spatial coordinates. Therefore, χ combines the effects of 1) variable, inaccurately known GS, 2) scattering, and 3) anelastic attenuation.

Because G_0 in eq. (3) is the fixed (reference, or background) value, all information about the seismic attenuation is contained in the frequency dependence of χ in eq. (1). In today's observations (Morozov, 2008, 2009a, 2010a, b), only a frequency-independent Q_e can typically be measured, and therefore we only have two observable parameters (γ and Q_e) to constrain the three physical factors associated with attenuation

(which are the GS, scattering, and anelastic attenuation). Consequently, one of these factors remains inherently unconstrained, and as argued by Morozov (2008, 2009a and 2010a), this factor is the scattering. Note that "scattering" as a part of wave propagation through a structure can only be identified subjectively, by the observer's treatment of a part of this structure as "random" or as a "perturbation" of some selected background[1].

Thus, we can only talk unambiguously about the frequency-independent (γ) and frequency-dependent (Q_e^{-1}) parts of χ and not about the GS and anelastic contributions to it *per se*. The entire anelastic attenuation should be included in Q_e^{-1}, because its effect should vanish at $f \to 0$, whereas the GS can generally contribute to both γ and Q_e^{-1}. However, for simplicity, in the spirit of the conventional frequency-independent GS models, we often interpret γ as the "residual GS" (Morozov, 2008, 2010a).

Third, transformation (2) implicitly assumes that $\chi \to 0$ as $f \to 0$, and therefore $\gamma = 0$ in (1). However, this limit is only valid when the GS is perfectly corrected for, which is never achieved in practice. Consequently, the quality factor Q derived from eq. (2) is unstable in respect to GS corrections (particularly in lower-frequency observations; Morozov, 2008), and when $\gamma > 0$, Q tends to increase with frequency. By contrast, when using the $\chi(f)$ directly, we are not limited by this constraint, and the interpretation is stable.

---

[1]The conservation of total elastic energy provides another distinction between the scattering and anelastic attenuation. However, this distinction is extremely difficult to employ in practical observations. Moreover, the conservation of energy is violated in popular modeling approaches, such as the Born approximation to scattering.

The temporal attenuation coefficient should generally be estimated directly from the seismic-amplitude data. However, if the amplitudes are not available, as in the present study, χ can be reconstructed from Q by using the inverse of (3): $\chi = \pi f Q^{-1}$. According to eq. (1), interpreting the $\chi(f)$ dependencies consists of plotting them in linear frequency scales and establishing their linearity (or non-linearity) with frequency. Unfortunately, this simple analysis is almost never performed in attenuation studies. In the following application to local-earthquake coda data, we will use such $\chi(f)$ dependencies to answer four questions: 1) whether they can be considered as linear in f as in eq. (1), 2) if so, whether non-zero intercept values $\gamma = \chi|_{f \to 0}$ are indicated by the data, 3) whether both γ and Q_e depend on the times of observations, and 4) what these variations suggest about the temporal variations and spatial distributions of the GS and anelastic attenuation within the subsurface.

3. Temporal variations of local-earthquake coda Q(f)

To illustrate the relation of $Q(f)$-type coda observations to $\chi(f)$, let us review the data from an aftershock study of an earthquake swarm along the San Andreas Fault (SAF) in central California. From July 17, 1973 to June 24, 1974, 185 earthquakes of magnitudes 0.9 to 3.3 were recorded at the temporary station STC located in Stone Canyon, approximately 1 km west of the SAF (Chouet, 1979). Note that the presence of such a major, linear crustal structure as the SAF zone in addition to the sedimentary and crustal layering makes this area particularly interesting for studying the effects of GS on attenuation measurements.

Figure 1a reproduces the frequency-dependent coda Q_c^{-1} from Aki (1980). The

observations were grouped into four time intervals: July 18 – September 11, 1973 (STC-1), September 12 – November 10, 1973 (STC-2), November 11, 1973 – February 10, 1974 (STC-3), and February 11 – June 24, 1974 (STC-4). From these data, Q_c^{-1} clearly increased at all frequencies sometime from mid-September to mid-October 1973 (Aki, 1980). However, beyond this general observation, more detailed variations of attenuation are difficult to analyze from this plot. Chouet (1979) and Aki (1980) described this change as intriguing but unclear and broadly attributed it to some rapid but strong variations of lithospheric heterogeneity (*i.e.*, Q_s^{-1}) within a large volume (tens of kilometres radius) of the lithosphere.

However, re-plotting the same data in terms of $\chi = \pi f Q^{-1}$ reveals linear attenuation patterns showing more detailed relationships between the datasets (Figure 1b). These patterns show that the convergence of all the $Q^{-1}(f)$ curves near ~25 Hz (Figure 1a) is incidental and principally related to dividing the values of χ by the frequency. By contrast, comparison of the intercepts and slopes of the attenuation-coefficient trends (dashed lines in Figure 1b), shows that: 1) GS factors are slightly below $\gamma \approx 0.04$ s^{-1} for STC-1 and about 0.05–0.06 s^{-1} for STC-2 through STC-4; 2) attenuation factor values are much higher than Q_c, with $Q_e \approx 10{,}000$ for STC-1 dropping to $Q_e \approx 3000$–4500 for STC-2 through STC-4. Such relatively high γ values appear characteristic for central California (Morozov, 2010a). At the same time, the values of Q_e appear unusually high (the previously observed value was $Q_e \approx 1250$; Morozov, 2010a), which may indicate a well-consolidated crust in the Stone Canyon area.

The observed linear $\chi(f)$ dependencies are reasonable within a roughly estimated

10% error on χ (Figure 1b, inset). Unfortunately, full estimation of errors in χ measurements requires revisiting the raw amplitude data, which is not available in this study. Chouet (1979) reported errors in $Q_c(f)$ at ~1–3% levels, which were similar to error estimates in many other studies. However, such error estimates only correspond to measuring the logarithmic decrements of r.m.s. amplitudes across ~30-s long time intervals. Such amplitudes are recorded at fixed points and filtered within narrow frequency bands, and consequently their slopes are nearly exponential and well defined. Apart from the time decay, coda amplitudes are also affected by the spatial and frequency amplitude variations (*e.g.*, resonances, tuning), which are apparent from the systematic amplitude variations in Figure 1b. Note the "spectral scalloping" resulting in systematically reduced amplitudes at 1.5, 6 (with one exception for STC-1), and 24 Hz and increased at 3 and 12 Hz in all recordings (Figure 1b). Because of such amplitude variations, the scatter of the resulting Q is much stronger than could be expected from Aki's (1969) model with ~1–3% errors in Q_c (see Figure 3).

The uncertainties in the resulting (γ, Q_e) values can be examined by using the linear regression analysis. Figure 2 shows cross-plots of (γ, Q_e) for the four time intervals, with their optimal parameter values shown by diamonds and areas of likelihood levels exceeding e^{-2} contoured. The stronger amplitude oscillations at lower frequencies (Figure 1b) cause most of the errors for STC-1 and STC-2 periods (Figure 2a). By excluding these frequencies, significantly tighter estimates of γ and Q_e can be obtained (Figure 2b). However, dropping the single 1.5-Hz reading for STC-1 shows that its Q_e^{-1} can in fact be set equal to zero (Figure 2b), which means that the attenuation in this interval may be too low to be detectable.

With either using the frequencies below 6 Hz or not, the variations of attenuation parameters with observation time are well-constrained, particularly in terms of γ (Figure 2). The attenuation increases from STC-1 to STC-3 and then reduces to STC-4.

To compare the relative levels of the GS and Q_e^{-1} contributions to attenuation, "cross-over" frequency $f_c = \gamma Q_e / \pi$ can be used (Morozov, 2008). For observation frequencies $f < f_c$ the GS dominates the anelastic attenuation, and at $f > f_c$, the Q_e^{-1} is dominant. In the present dataset (for example, for STC-2), $f_c \approx 86$ Hz, which is far above the observation frequency band. Therefore, the effect of GS dominates that of Q_e^{-1} within all time intervals and at all frequencies (Figure 3). It appears that the "geometrical" effect is the main cause of both the apparent coda Q_c attenuation and of its temporal variation.

By correlating the temporal trends of γ and Q_e to χ_c values derived from Q_c at $f = 24$ Hz given by Chouet (1979), we can further evaluate the significance of these trends (Figure 3). Despite their wide scatter, the individual χ_c data appear consistent with the inferred temporal trends. Notably, there actually appears to be no increase in χ_c until the start of the rainy season on October 7, 1973 (Figure 3). Therefore, contrary to the conclusion by Aki (1980), it is still likely that the increase of both γ and Q_e^{-1} was associated with a change in the near-surface conditions caused by the rain.

Three significant differences of our empirical $\chi(f)$ model compared to Aki's (1969) coda scattering model allow us to look for the source of coda in the near subsurface. First, as determined above, the GS factor γ dominates coda attenuation at Stone Canyon, and scattering within a large volume of the lithospere is not required for its explanation. GS is most sensitive to the near-surface structure, where the strongest

velocity contrasts and reflectivities are present. Numerical waveform modeling (Morozov *et al*., 2008) showed that introduction of a low-velocity, high-attenuation layer in the upper crust can significantly increase coda γ, and therefore the effect of rising water table could be qualitatively consistent with the observed increase of γ (Figure 3). Second, in our model, values of Q_e are significantly higher (3000–10,000 compared to 100–1000 by Chouet, 1979), and this smaller amount of attenuation could be attributed to the upper crust. Third, the attenuation factor Q_e^{-1} is frequency-independent, and therefore it does not require scattering and could be caused by anelastic losses in wet and weathered near-surface layers.

4. Temporal change in coda attenuation during 1981 Mount St. Helens eruption

Another interesting example of temporal variations of coda attenuation was given by Fehler *et al*. (1988). Three groups of measurements were conducted at Mt. St. Helens: prior to the September 3–6, 1981 eruption, during the eruption, and after it. In the coda quality-factor form, the attenuation (Q_c^{-1}) relatively weakly varied with frequency within each of these intervals and decreased by 20–30% after the eruption (Figure 4a). Fehler *et al*. (1988) noted the peak in Q_c^{-1} near 10 Hz and suggested that it could be analogous to the peak at 0.5 Hz hypothesized by Aki (1980) for non-volcanic regions. Aki (1980) interpreted this peak as caused by scattering and estimated the corresponding scale-length of lithospheric heterogeneity as ~4km. Following the same argument, Fehler *et al*. (1988) suggested that a heterogeneity scale-length of ~500 m could be responsible for the 10-Hz Q_c^{-1} peak at Mount St. Helens.

However, if we do not assume scattering from the very beginning but re-plot the same data in the χ_c form, a different interpretation is revealed (Figure 4b). Above ~18 Hz, $\chi_c(f)$ shows linear patterns similar to those in Figure 1. Their intercept values of $\gamma \approx 0.18$ s^{-1} are 3–4 times higher than those in Figure 1, likely because of the stronger positive GS (defocusing) caused by the cone of the volcano. Similarly to the case of Figure 1 (somewhat less dramatically), the effect of the "material" attenuation ($\pi f Q_e^{-1}$) represents only about a half of the observed coda attenuation, and the rest is represented by the residual GS.

An "absorption peak" is present in the apparent Q_c^{-1} near 10 Hz (Figure 4a); nevertheless, the attenuation is not actually increased at this frequency (Figure 4b). This frequency corresponds to Q_e^{-1} starting to decrease and γ changing from negative to positive, which can be noted by extrapolating the linear $\chi_c(f)$ trends (Figure 4b). This transition can be explained by switching from predominantly surface waves constituting the coda below ~10–15 Hz to mostly body waves above these frequencies. Such relative reduction of the high-frequency surface-wave amplitudes is well known in reflection seismology and explained by the near-surface attenuation. When a single spherical-wave GS correction is used at all frequencies, surface waves become over-corrected (*i.e.,* focused, with $\gamma < 0$; Morozov, 2009a and 2010b) and body waves from the upper-crustal sources — under-corrected (defocused, $\gamma > 0$; see Morozov, 2010a).

Interestingly, the pre-eruption GS value of $\gamma \approx 0.18$ s^{-1} increased to ~0.25 s^{-1} during the eruption and returned to its original value afterwards (dashed grey lines in Figure 4b). This return to the original value could be expected if γ were a property of the

structure (such as the shape of the mountain and its subsurface), which generally resumed its original state. The co-eruptive increase of γ could be related to the inflation of the cone of the volcano (Dzurisin *et al*., 1981). Attenuation decreased from $Q_e \approx 400$ before the eruption to ~750 after it (Figure 4b). This change could be explained by the removal of gas and magma from the volcano chambers and the corresponding reduction of anelastic attenuation. Note that this is a significantly stronger change (~50%) compared to the 20–30% change in the apparent Q_c^{-1}. At the same time, the values of Q_e are about twice larger than those of Q_c (Figure 4b), and therefore a smaller volume of attenuative material needs to be removed in order to account for this change.

The character of the co-eruptive $\chi_c(f)$ curve in Figure 4b is less clear, suggesting an increase in both γ (which is likely true to some extent, due to cone inflation) and Q_e to ~1400. The latter value Q_e appears to be somewhat too high, considering the level of Q_e ≈750 after the eruption and the average crustal $Q_e \approx$ 1000–1100 (Morozov, 2008). Three possible reasons could lead to increased values of both of these parameters: 1) migration of the earthquake sources to the top of the mountain during the eruption, 2) increased high-frequency noise during the eruption, causing over-estimated Q_c values, and 3) reduction of tremor amplitudes below ~25 Hz, which would appear as an increase in χ (compare to the "spectral scalloping" in Figure 1). The last two of these reasons are similar and appear plausible, judging by the near-constant values of χ_c at 20–40 Hz during the eruption (Figure 4b). These and other explanations could be examined further by revisiting the raw data and by modeling, which is, however, outside of the scope of this paper.

5. Discussion

The above analysis shows that the temporal attenuation coefficient χ contains more information than usually recovered by its conversion into the conventional Q form. Attenuation-coefficient plots allow grouping the observed dependencies into consistent, often linear, patterns and provide wider and clearer separations between responses from different structures. Parameters of such responses can be measured quantitatively and irrespectively of the assumed GS and theoretical models. The resulting measurements reveal additional detail in the attenuation patterns and allow detection of temporal variations in GS and Q that were not noticed before.

Scattering certainly represents the principal mechanism of seismic coda generation, and numerous efforts have been made for developing scattering-based coda models (Aki, 1969; Aki and Chouet, 1975; Dainty and Toksöz, 1977; Aki, 1980; Roecker *et al*., 1982; Aki, 1991; Hoshiba *et al*., 1991; Zeng *et a*l., 1991; Fehler *et al*., 1992; Hoshiba, 1993; Paasschens, 1997; Chouet, 2003; Carcolé and Ugalde, 2008). However, in the author's opinion, model-based approaches will unlikely reach the accuracy required for unambiguous inversion for the *in situ Q*, and even more so – of its frequency dependence. Before the observed coda amplitudes can be interpreted in terms of the scattering parameters (*i.e*., scale lengths of heterogeneities, opening and closing of micro-cracks, *etc*.), many factors of the structure need to be accounted for, such as: (a) 3-D geometry, including major reflecting boundaries, free-surface topography, sedimentary layering, and fault zones; (b) vertical stratification, which causes bending and reflecting rays, variations of reflection amplitudes with incidence angles, and tuning effects; (c) anelastic attenuation, and (d) source and receiver directivities. In real-Earth problems and

at seismological frequencies, these factors should be superior to the elastic scattering on random, small-scale heterogeneities. If scattering is still required after these factors are accounted for, then the next critical factors to consider are: (e) spatial distribution of scatterers (such as their proximity to the surface), and (f) their magnitudes and scale-lengths. Unfortunately, in a model-based approach, factors (a) – (e) are practically intractable with the existing datasets and limited knowledge of the lithospheric structure. Nevertheless, this still does not mean that these factors can be ignored for simplicity and a uniform-space, isotropic scattering model with the only factor (f) used instead.

Despite the difficulties of the model-based approach, attenuation data can be readily interpreted phenomenologically, as described in Morozov (2008) and in this paper. The linearity of $\chi(f)$ dependencies becomes a strong observational fact guiding the interpretation. This fact suggests that the underlying physical processes could also be linear in f, *i.e*. that the *in situ* Q is frequency-independent within the measured frequency band (1.5–25 Hz in Figure 1b and 18–40 Hz in Figure 4b). This fact should not be overshadowed by the frequency dependence of the apparent Q_c. By its definition, Q_c essentially only gives a standard form for representing the time-domain coda shapes. In our examples (Figures 1 and 4a), a strongly frequency-dependent Q_c was mostly caused by the residual GS, which also appeared to be the case in other observations (Morozov, 2008, 2010a, b). Intuitive association of this quantity with physical parameters of the medium (such as the temperature, pressure, fluids, density of fractures) should be done with caution.

Similarly to Q_c, Q_e is also an "apparent" property that still needs to be inverted for the local physical parameters of the medium. Frequency independence of Q_e observed in

many examples suggests its relation to the anelastic Q of the medium. This can be seen from the symmetry with which we treat the residual GS and Q^{-1} in our approach. Consider the following expression for the cumulative attenuation factor t^* as an integral of the *in situ* Q^{-1} along the "wave path" (Der and Lees, 1985):

$$t^* = \int_{path} Q^{-1} d\tau , \tag{4}$$

where τ is the travel time measured from 0 to t. Quantity t^* is prone of the same type of instability as Q^{-1} ($t^* \propto f^1$; Section 2), yet noting that $\chi t = t^* f$ in eq. (3), we can generalize this path average to

$$\chi = \frac{1}{t} \int_{path} \chi_i d\tau , \tag{5}$$

where χ_i becomes the "intrinsic" attenuation coefficient, which incorporates the effects of anelastic attenuation and local (small-scale) scattering. Thus, χ_i is quite similar to the traditional *in situ* Q^{-1} in the sense that it can be averaged over wave paths to predict the logarithms of seismic amplitudes. Similarly to the apparent χ in eq. (1), χ_i can be decomposed into the frequency-independent and dependent parts:

$$\chi_i(f) = \gamma_i + \frac{\pi}{Q_i} f , \tag{6}$$

which can be interpreted as the GS perturbation per unit travel time (γ_i) and the combined anelastic/scattering attenuation (Q_i^{-1}), respectively. Quantity Q_i was referred to as the "material" Q throughout this paper. If the wave paths are frequency-independent, then these properties are also accumulated along the paths to yield the corresponding apparent

quantities:

$$\gamma = \frac{1}{t}\int_{path} \gamma_i d\tau \text{, and } Q_e^{-1} = \frac{1}{t}\int_{path} Q_i^{-1} d\tau \text{.} \quad (7)$$

Although this is only a phenomenological approximation, it shows that GS perturbations are accumulated during wave propagation in the same manner as anelastic attenuation. Without attempting a rigorous derivation, note that for refractions in a smooth medium, γ_i represents the additional local wavefront curvatures in respect to the reference background GS (Morozov, 2010d). For a medium with short-scale heterogeneities, γ_i is proportional to the mean squared reflection amplitude (*ibid*).

From geological considerations, the largest values of both γ_i (low velocities, high gradients, and strong reflectivity) and Q_i^{-1} (high attenuation) should be concentrated in the near surface and/or near the magma chambers, conduit and cone of the stratovolcano. The same areas are most likely to be affected by rapid changes in the environmental conditions, such as seasonal variations or eruptions. Because of the relatively small changes in the observed γ and Q_e^{-1} and high contrasts in γ_i and Q_i^{-1}, only a small portion of the crust needs to be affected by such changes in order to produce the observed effects. For example, with Q_e changing from 10,000 to 3000 and typical values of Q_i in wet near-surface sediments of 10–20, only 0.3 to 0.7% of the total ray path beneath the station needs to be affected by the increased attenuation (eq. (7); Figure 5). Similar estimates should apply to the molten lava, gas, and water beneath the volcano. Note that low-velocity near-surface layers (and presumably also the volcanic conduit and cone) provide efficient waveguides for trapping numerous guided wave modes known as “ground roll” in reflection seismology. Ground roll scattered from surface topography and near-surface

heterogeneities is commonly observed as characteristic criss-crossing patterns in seismic records. All this shows that the near surface could be the main region where both scattering of coda waves and their attenuation occurs.

A good quantitative approximation for the realistic coda model can be obtained by considering scattering as occurring near the free surface (Morozov and Smithson, 2000; Morozov *et al*., 2008). The free surface (including topography, weathered zone, and maybe sedimentary sequences) represents by far the strongest reflector package, which also contains the strongest attenuation and is traversed by all waves reaching the receivers (Figure 5a). In volcanic environments, the magma source region is also characterized by low velocities, high attenuation, and extreme complexity that enhances scattering (Chouet, 2003; Lin *et al*., 2005). Thus, the principal difference of volcanic settings appears to be in a greatly enlarged zone of heterogeneity, in which both the sources and areas of temporal variations may be located (Figure 5b).

The above difference in the shapes of high-χ_i structures explains the differences in the observed characters of temporal changes of γ and Q_e in the two cases considered here (Figures 1b and 4b). It appears that in the volcanic case (disregarding the co-eruptive phase), the change occurred within the subsurface and consisted in the removal of the low-Q_i gas and magma, which led to a reduction in Q_e^{-1}. At the same time, γ_i remained unchanged because the ray shapes did not change neither near the source nor the receiver (Figure 4b). By contrast, in the non-volcanic case (Figure 1b), we interpreted the change as related to seasonal precipitation, which occurred near the opposite (receiver) end, where the zone of strongest scattering was also located. Therefore, the high-γ_i, high-Q_i^{-1} near-surface layer affected both the resulting γ and Q_e^{-1}, as shown in

Figures 1b to 3. An additional difference was in the observed seasonal cycle in Figure 3 being incomplete; with longer recording, both γ and Q_e^{-1} in this case might return to the original values.

Conclusions

Abandoning the preconceived uniform-scattering coda models early in the interpretation reveals linear dependencies of the temporal attenuation coefficient, χ, on frequency in local-coda observations. This linearity allows us to measure two new parameters, γ and Q_e, which are associated with the geometrical spreading and local material attenuation, respectively. Although generally recognising scattering as the principal mechanism of coda formation, we observe that:

1) The residual geometrical spreading, γ, which is usually disregarded in the conventional single- or multiple-scattering models, has the greatest effects on both coda attenuation levels and their temporal variations;

2) With the use of Q_e, values of Q were significantly updated (usually increased) and become frequency-independent; and

3) Scattering and temporal changes appear to occur in significantly more compact and shallow areas than usually thought. These areas are also likely affected by the changes in the environment. The previously inferred but hitherto poorly explained strong and rapid changes in velocity heterogeneity within tens of thousand of cubic kilometres are not required to explain neither the coda properties nor its temporal variations.

The above conclusions were illustrated on two case studies of the temporally-variant local-earthquake coda Q_c: in a non-volcanic (Stone Canyon in central California) and volcanic areas (Mt. St. Helens, Washington). In both cases, the effects of γ on coda attenuation were significantly stronger than those of Q_e^{-1}. At Stone Canyon, γ ranged from 0.035 to 0.06 s^{-1} and Q_e varied from 3000 to 10,000, with γ increasing and Q_e decreasing during the winter season. At Mt. St. Helens, $\gamma \approx 0.18$ s^{-1}, and Q_e varied from 400 before the eruption to 750 after it. The observed temporal variations were explained by the near-surface effects, related to seasonal variations in the non-volcanic case and magma-, gas-, and geothermal-system variations in the volcanic case. The effects of attenuation were also much weaker ($Q_e^{-1} << Q_c^{-1}$) than those expected by attributing the values of Q_c to the subsurface. Scattering was interpreted as occurring near the surface or near the volcano conduit, where both the velocity heterogeneity and attenuation should be the strongest. Scattering attenuation (Q_s^{-1}) did not appear to be a significant factor in these areas, or at least it was not required by the data and unconstrained due to a fundamental ambiguity of this quantity.

Acknowledgements

This study was supported by NSERC Discovery Grant RGPIN261610-03. GNU Octave software (Octave, 2009) was used for computations, and GMT programs (Wessel and Smith, 1995) – for preparation of illustrations.

References

Aki, K., 1969. Analysis of the seismic coda of local earthquakes as scattered waves, J. Geophys. Res., 74, 615–631.

Aki, K., 1980. Scattering and attenuation of shear waves in the lithosphere, J. Geophys. Res. 85: 6496-6504.

Aki, K., 1991.Summary of discussions on coda waves at the Istanbul IASPEI meeting, Phys. Earth Planet. Int., 67, 1–3.

Aki, K., Chouet, B., 1975. Origin of coda waves: source, attenuation, and scattering effects, J. Geophys. Res., 80, 3322–3342.

Aki, K., Richards P.G., 2002. Quantitative Seismology, Second Edition, University Science Books, Sausalito, CA.

Carcolé, E., Ugalde, A., 2008. Formulation of the multiple non-isotropic scattering process in 2-D for non-spherical source radiation, Geophys. J. Int., 174, 1037–1051.

Chernov, L.A., 1960. *Wave Propagation in a Random Medium*, McGraw-Hill, New York, 168pp.

Chouet, B., 1976. Source, scattering, and attenuation effects on high frequency seismic waves, Ph.D. dissertation, Mass. Inst. of Technol., Cambridge, MA.

Chouet, B., 1979. Temporal variation of earthquake coda near Stone Canyon, California, Geophys. Res. Lett., 6,143–146.

Chouet, B., 2003. Volcano seismology, Pure Appl. Geophys., 160,739–788.

Dainty, A.M., 1981. A scattering model to explain seismic *Q* observations in the lithosphere between 1 and 30 Hz, Geophys. Res. Lett., 8, 1126–1128.

Dainty, A.M., Toksöz, M.N., 1977. Elastic wave propagation in a highly scattering medium – A diffusion approach, J. Geophys., 43: 375–388.

Del Pezzo, E., Bianco, F., Petrosino, S., Saccorotti, G., 2004. Changes in the coda decay rate and shear-wave splitting parameters associated with seismic swarms at Mt. Vesuvius, Italy, Bull. Seismol. Soc. Am., 94, 439–452.

Der, Z.A., Lees, A.C., 1985. Methodologies for estimating $t^*(f)$ from short-period body waves and regional variations of $t^*(f)$ in the United States, Geophys. J. R. Astr. Soc., 82: 125–140.

Dzurisin, D., Johnson, D.J., Westphal, J.A., 1981. Ground tilts during two recent eruptions of Mount St. Helens, Washington, Eos, Transactions, American Geophysical Union, 62, 1089.

Fehler, M., Hoshiba, M., Sato, H., Obara, K., 1992. Separation of scattering and intrinsic attenuation for the Kanto-Tokai region, Japan, using measurements of *S*-wave energy versus hypocentral distance, Geophys. J. Int., 108, 787–800.

Fehler, M., Roberts, P., Fairbanks T., 1988. A temporal change in coda wave attenuation observed during an eruption of Mount St. Helens, J. Geophys. Res., 93, 4367–4373.

Gusev, A.A., 1997. Temporal variations of the coda decay rate on Kamchatka: Are they real and precursory? J. Geophys. Res., 102, 8381–8396.

Hoshiba, M., 1993. Separation of scattering attenuation and intrinsic absorption in Japan using the Multiple Lapse Time Window Analysis of full seismogram envelope, J. Geophys., Res., 98, 15,809–15,824.

Hoshiba, M., Sato, H., Fehler, M. 1991. Numerical basis of the separation of scattering

and intrinsic absorption from full seismogram envelope: a Monte-Carlo simulation of multiple isotropic scattering, Pap. Meteorol. Geophys., 42, 65–91.

Jin, A., Aki, K., 1986. Temporal change in coda *Q* before the Tangshan earthquake of 1976 and the Haicheng earthquake of 1975, J. Geophys. Res., 91, 665–673.

Kinoshita, S., 1994. Frequency-dependent attenuation of shear waves in the crust of the southern Kanto area, Japan, Bull. Seism. Soc. Am., 84, 1387–1396.

Lin, C.-H., Konstantinou, K. I., Pu, H.-C., Hsu, C.-C., Lin, Y.-M., You, S.-H., Huang, Y.-P., (2005), Preliminary results from seismic monitoring at the Tatun volcanic area of northern Taiwan, Terr. Atm. Ocean. Sci. (TAO), 16, 563–577.

Londono, J.M., 1996. Temporal change in coda *Q* at Nevado Del Ruiz Volcano, Colombia, J. Volcan. Geotherm. Res., 73: 129–139.

Mitchell, B., 2010. Prologue and invitation to participate in a forum on the frequency dependence of seismic *Q*, Pure Appl. Geophys. 167, 1129, doi: 10.1007/s00024-010-0180-3

Moncayo, E., Vargas, C., Durán, J. 2004. Temporal variation of coda-*Q* at Calderas volcano, Colombia, Earth Sci. Res. J., 8, 19–24.

Morozov, I.B., 2008. Geometrical attenuation, frequency dependence of *Q*, and the absorption band problem, Geophys. J. Int., 175, 239–252.

Morozov, I.B., 2009a. Thirty years of confusion around "scattering *Q*"? Seismol. Res. Lett., 80, 5–7.

Morozov, I. B., 2009b. Reply to "Comment on 'Thirty years of confusion around 'scattering *Q*'?'" by J. Xie and M. Fehler, Seismol. Res. Lett., 80, 648–649.

Morozov I.B., 2009c. On the use of quality factor in seismology. Eos Trans. AGU

90(52), Fall Meet. Suppl., Abstract S44A-02.

Morozov, I.B. 2010a, On the causes of frequency-dependent apparent seismological *Q*. Pure Appl. Geophys. 167, 1131–1146, doi: 10.1007/s00024-010-0100-6

Morozov, I.B. 2010b, Attenuation coefficients of Rayleigh and *Lg* waves, J. Seismol. 14, 803-822, doi: 10.1007/s10950-010-9196-5

Morozov, I.B. 2010c, Anelastic acoustic impedance and the correspondence principle, Geophys. Prosp., doi 10.1111/j.1365-2478.2010.00890.x

Morozov, I.B. 2010d, Seismological attenuation coefficient and *Q*, Seism. Res. Lett. 81, 307.

Morozov, I.B., Smithson, S.B. 2000. Coda of long-range arrivals from nuclear explosions, Bull. Seism. Soc. Am., 90, 929–939.

Morozov, I.B., Zhang, C., Duenow, J.N., Morozova, E.A., Smithson, S., 2008. Frequency dependence of regional coda *Q*: Part I. Numerical modelling and an example from Peaceful Nuclear Explosions: Bull. Seism. Soc. Am., 98, 2615–2628, doi: 10.1785/0120080037

Novelo-Casanova, D.A., Berg, E., Hsu, V., Helsley C.E., 1985. Time-space variation of seismic *S*-wave coda attenuation (Q^{-1}) and magnitude distribution (*b*-values), Geophys. Res. Lett., 12: 789-792.

Novelo-Casanova, D. A., Martinez-Bringas, A., Valdés-González C., 2006. Temporal variation of Q_c^{-1} and *b*-values associated to the December 2000 – January 2001 volcanic activity at the Popocapetl volcano, Mexico, J. Volcanol. Geotherm. Res. 152, 347–358.

Octave, 2009. http://www.gnu.org/software/octave/about.html, accessed November 8,

2009.

Paasschens, J.C.J., 1997. Solution of the time-dependent Boltzmann equation, Phys. Rev. E, 56, 1135–1141.

Peng, J.Y., Aki, K., Chouet, B., Johnson, P., Lee, W.H.K.. Marks, S., Newberry, J.T., Ryall, A., Stewart, S., and Tottingham, D. M., 1986. Temporal change in coda *Q* associated with the Round Valley, earthquake of November 23, 1984, J. Geophys. Res., 92, 3507–3526.

Rhea, S. 1984. *Q* determined from local earthquakes in the South Carolina coastal plain, Bull. Seismol. Soc. Am., 74, 2257–2268.

Roecker, S.W., Tucker, B., King, J., Hatzfeld, D. 1982. Estimates of *Q* in central Asia as a function of frequency and depth using the coda of locally recorded earthquakes, Bull. Seismol. Soc. Am., 72, 129–149.

Sato, H., 1978. Mean free path of *S* waves under the Kanto district of Japan, J. Phys. Earth, 26, 185–198.

Sato, H., 1986. Temporal change in attenuation intensity before and after the eastern Yamanashi earthquake of 1983, in central Japan, J. Geophys. Res., 91, 2049–2061.

Sato, H., 1986. Temporal change of scattering and attenuation associated with the earthquake occurrence – a review of recent studies in coda waves, Pure Appl. Geophys., 126, 465–497.

Stewart, R.R., Toksöz, M.N., Timur A., 1983. Strain dependent attenuation: observation and a proposed mechanism, J. Geophys. Res., 88, 546–554.

Wessel P., Smith, W.H.F., 1995. New version of the Generic Mapping Tools released:

EOS Trans. Am. Geophys. U., 76, 329.

Xie, J., Fehler, M., 2009. Comment on 'Thirty years of confusion around 'scattering *Q*'?' by Igor B. Morozov, Seismol. Res. Lett., 80, 646–647.

Xie, J., 2010, Can we improve estimates of seismological Q using a new ''geometrical spreading'' model? Pure Appl. Geophys. 167, 1147–1162, doi: 10.1007/s00024-010-0188-8

Zeng, Y., Su, F., Aki, K., 1991. Scattered wave energy propagation in a random isotropic scattering medium, I, Theory, J. Geophys. Res., 96, 607–619.

Figures

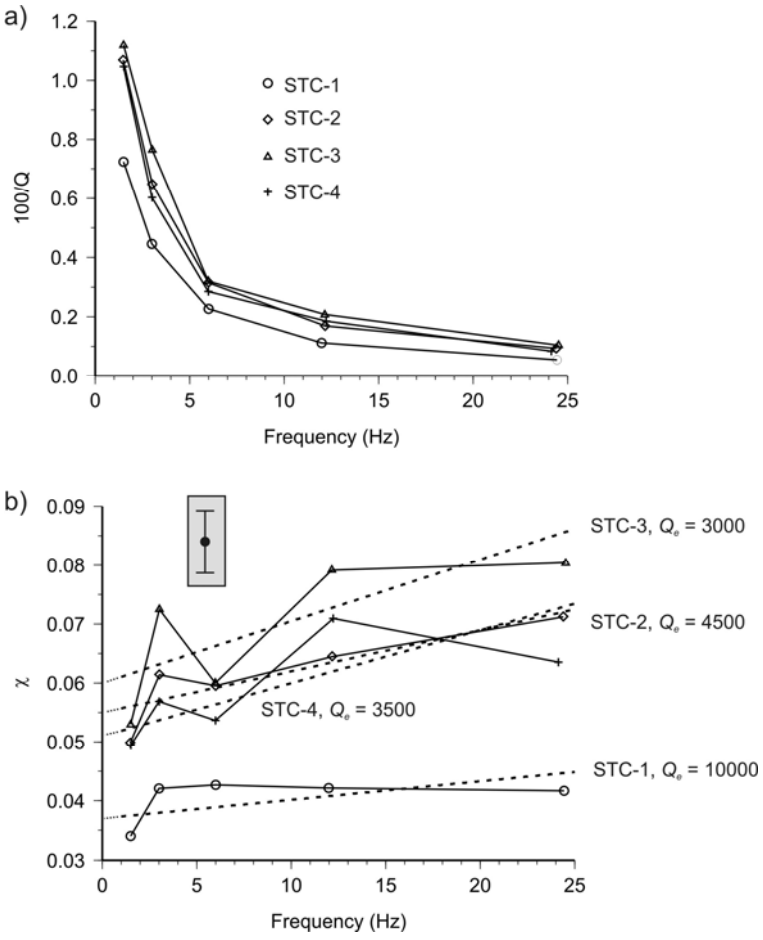

Figure 1. Frequency dependence of local-earthquake coda attenuation at Stone Canyon (California) station from Aki (1980). Labels indicate the consecutive time intervals. a) Data in $100/Q$ form, as in Aki (1980). b) The same data in $\chi(f)$ form. Note that the separation of periods STC-2 through STC-4 is much clearer, and $\chi(f)$ shows linear dependencies on f (dashed lines; Q_e values given in labels). A reference 10% error bar on χ is shown in inset.

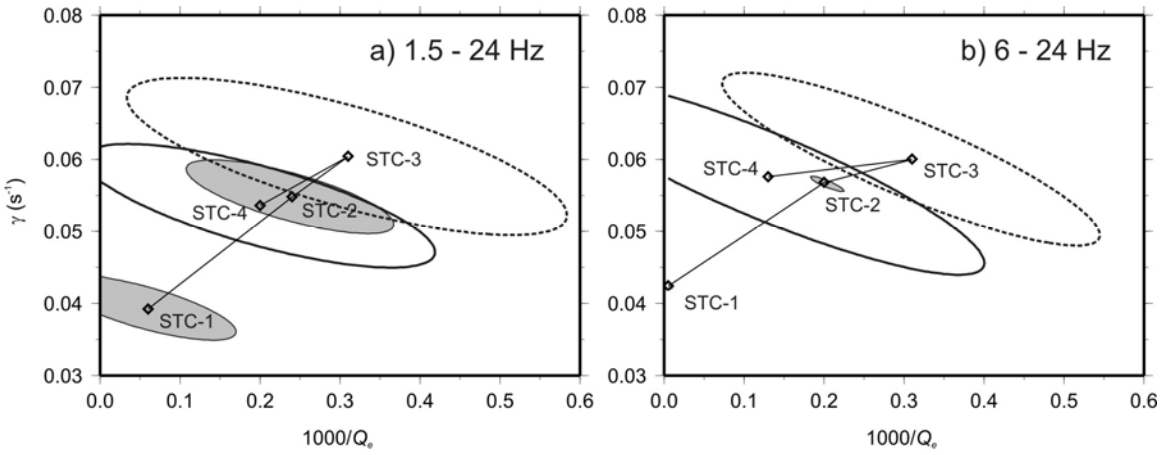

Figure 2. (γ, Q_e^{-1}) cross-plots corresponding to linear $\chi(f)$. Ellipses indicate areas of squared data misfit less than twice higher than for the optimal (γ, Q_e) values (diamonds). a) Fitting using the entire 1.5–24 Hz frequency band; b) using frequencies 6 – 24 Hz. Note the temporal trends in both γ and Q_e (lines).

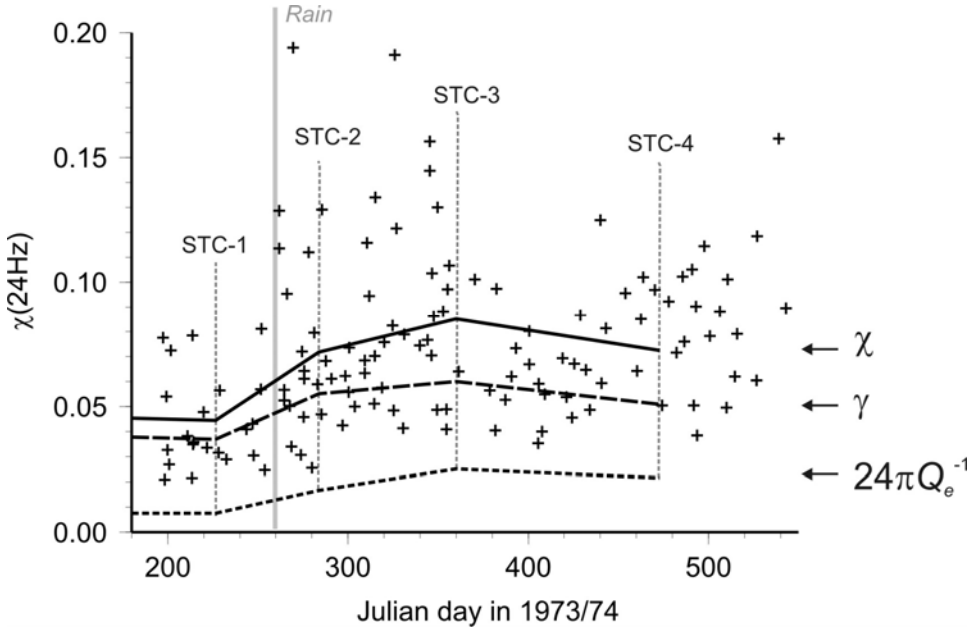

Figure 3. Temporal variations of local-coda χ in Stone Canyon at 24 Hz. Crosses are coda data from Chouet (1979), and black lines show the interpreted γ values (dashed), contribution from Q_e^{-1} (short dash), and total χ (solid) from Figure 1. Grey lines indicate middles of measurement intervals (dashed) and the start of rainy season (October 7, 1973; Aki, 1980).

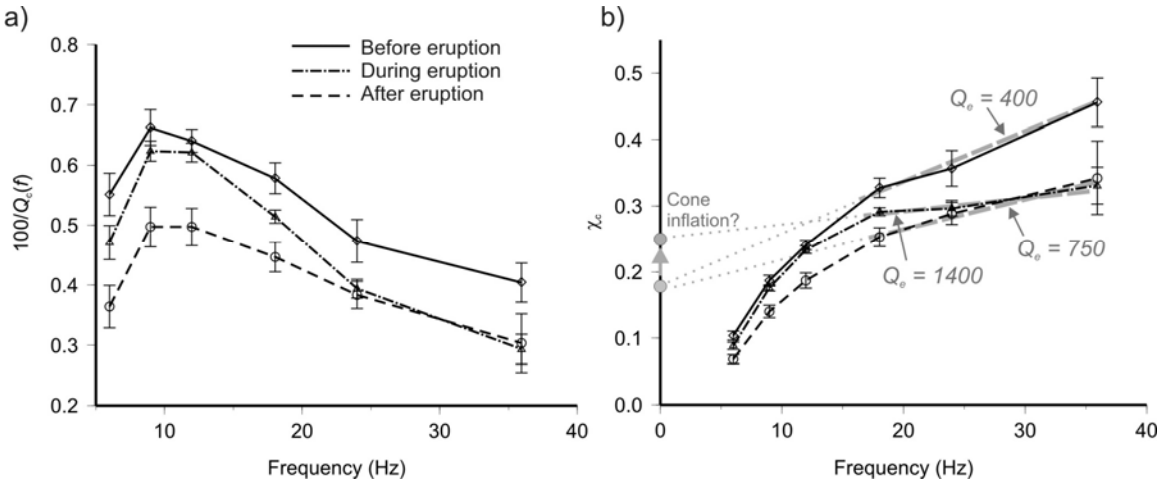

Figure 4. Coda attenuation data at Mount St. Helens. a) $Q_c^{-1}(f)$ data (Fehler *et al*., 1988). Note the peak at 10 Hz and decreasing Q_c^{-1} after the eruption. b) The same data in $\chi_c(f)$ form. Dashed grey lines show the interpreted linear trends in $\chi_c(f)$. Note the linear $\chi_c(f)$ dependencies at $f >$ ~18 Hz, with slopes decreasing after the eruption.

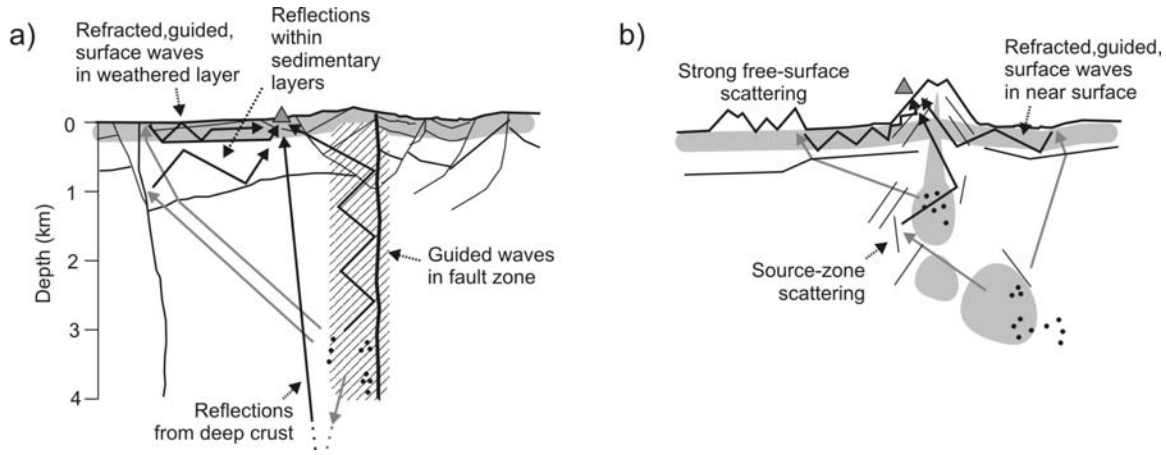

Figure 5. Schematic models of scattering responsible for coda formation: a) non-volcanic case (vicinity of San Andreas Fault); b) volcanic case. Grey indicates zones subject to rapid temporal variations. Black dots are the earthquakes, grey triangles represent seismic stations. Note that in both cases, scattering is concentrated near the free surface and potentially within other, relatively compact zones of increased heterogeneity.